Reaction Kinetics, Mechanisms and Catalysis (2019) 128:1127–1139
https://doi.org/10.1007/s11144-019-01677-8

Efficient catalytic photodegradation of methylene blue from medical lab wastewater using MgO nanoparticles synthesized by direct precipitation method

Bakhtyar K. Aziz[1] · **Mozart A. H. Karim**[2]

Received: 4 August 2019 / Accepted: 18 September 2019 / Published online: 25 September 2019
© Akadémiai Kiadó, Budapest, Hungary 2019

Abstract

Methylene blue is the main component of several stains such as Wright–Giemsa and Leishman stain that are used in histology and hematology laboratories. 97.8% of methylene blue from medical laboratory wastewater were photodegraded with the aid of MgO nanoparticles as photocatalysts and direct solar irradiation as a renewable source. The rate of photodegradation was 0.0184 min^{-1}. The direct precipitation method was used as a simple and low cost method to synthesize MgO nanoparticles in the size range of 2.5–11.3 nm as estimated from X–ray diffraction peaks. The optical band gap energy was reduced to 4.25 eV. The photoluminescence spectra of MgO nanoparticles show four bands corresponding to F and F^+ oxygen vacancy defects. The effects of the operational parameters (MgO dose, initial pH, irradiation source energy, initial concentration of the dye and temperature) were evaluated on the efficiency and rate of the photodegradation. The efficiency of the synthesized MgO nanoparticles was compared with TiO_2 and ZnO nanoparticles as well.

Keywords MgO nanoparticles · Catalytic photodegradation · Medical lab wastewater · Blood film

Electronic supplementary material The online version of this article (https://doi.org/10.1007/s11144-019-01677-8) contains supplementary material, which is available to authorized users.

✉ Bakhtyar K. Aziz
bakhtyar.kamal@charmouniversity.org

[1] College of Medical and Applied Sciences, Charmo University, Peshawa Str, Chamchamal 46025, Iraq

[2] Chemistry Department, College of Science, University of Sulamani, Sulaimani 46001, Iraq

Introduction

Significant water pollution results from dye manufacturing industries from which 2% is lost and industrial finishing step of coloring products from which only a part of the dye is used and the rest of the dye entering rivers and lake through discharge [1]. Methylene blue (MB) is the main component of several stains, such as Wright–Giemsa stain, that are used in medical laboratories to demonstrate microscopic life in a brilliant color. It is also used to stain peripheral blood and bone marrow aspirate smears [2]. The presence of dyes in water is highly hazardous even in very low concentrations [3] and need to be treated, preferably on site before discharge to sewage, rivers and lakes. Ideal wastewater treatment should mineralize the dye completely to CO_2 and H_2O [4]. Conventional techniques used in the treatment of polluted water such as precipitation [5], adsorption [6], evaporation [7], or membrane filtration are powerful techniques [8]. These methods accumulate the pollutants or convert them from one phase to another but not destroying the pollutant. Among the destructive methods such as biodegradation [9], chemical oxidation [10], the catalytic photodegradation technique has attracted researchers to develop efficient and economic photocatalyst [11]. Catalytic photodegradation is a heterogeneous reaction with a solid phase acting as the light absorbing photocatalyst and a liquid or gaseous phase that contain the organic pollutant. A typical mechanism of photodegradation involve the excitation of electrons from the valence band (VB) to the conduction band (CB) of the photocatalyst and formation of holes in the VB which are designated as h_{vb}^{+}. The freely moving electron in the CB $\left(e_{cb}^{-}\right)$ and h_{vb}^{+} can either recombine and dissipate the absorbed photon energy as thermal energy, or reacts further to produce reactive species like hydroxyl radical ($OH^{\cdot}$) and superoxide ion $\left(O_2^{-}\right)$. These reactive species can oxidize organic molecules unselectively. TiO_2 is the most widely studied photocatalyst due to its high efficiency [12]. On the other hand, the overall process of catalytic photodegradation is governed by the operational parameters like catalyst dose, initial pH, initial concentration of the organic pollutant, temperature, and radiation intensity [3]. Solar radiation is a free natural source of radiation that have an average of 1366 W/m^2 power at the top of the atmosphere. Only one quarter of this power is reaching the earth surface (342 W/m^2) in sunny days [13]. TiO_2 is the most widely used photocatalyst. The high band-gap energy of TiO_2 (anatase $\approx$3.2 eV) is one of the main drawbacks of its application (UVA radiation is needed for TiO_2 activation) (5% of the solar energy) [14]. To overcome this drawback, metal ion doped (e.g., Au) and non-metal (e.g., N) doped TiO_2 were studied widely. TiO_2 has low affinity toward organic pollutants (hydrophobic pollutants) and hence low adsorption and slow rate of photodegradation which is another limitation of TiO_2 photocatalyst. Aggregate formation, difficulty in separation and recovery of the TiO_2 after photodegradation are further limitation of the TiO_2 applications [15]. Various metal oxides were used as dynamic photocatalyst materials for the degradation of organic contaminants [16] such as ZnO [17], TiO_2 [18], α-Fe_2O_3 [19], CuO [20], and WO_3 [21]. Magnesium oxide (MgO) has been widely used in various applications such as antibacterial material, refractory material in industry, and catalysis. MgO is a versatile metal oxide material, with

different properties like large band gap, excellent thermodynamical stability, low refractive index and low dielectric constant [22]. Surface properties such as surface area, porosity and surface morphology of MgO nanoparticles (MgO-NPs) plays a crucial role in determining its efficiency as a photocatalyst [23]. The surface properties of MgO-NPs and their morphology are largely determined by the method of synthesis, such as sol–gel [24] hydrothermal [25], sonochemical [26]. Most of the synthesis methods do not apply to industrial scale because they need high technology, high temperature and different chemicals as templates or surfactants [27]. The physical, chemical, electronic, optical and catalytic properties are much dependent on the size and shapes of the nanoparticles. Therefore, wide-bandgap metal oxide nanomaterials with controllable size and morphology became an interested field of research [28]. The controlled growth process is very important to obtain the desired particle size and morphology of the nanomaterial. The simplicity of the process makes it easier to be applied in an industrial scale. Direct thermal decomposition procedure was utilized to synthesize crystalline ZnO microflowers with excellent photocatalytic activity [29]. Direct precipitation method for the synthesis of MgO-NPs have several advantages such as simplicity in technology, one-step process, industrial scale production and low cost [30]. The complete separation of the photocatalyst (TiO_2, ZnO, etc.) is one of the disadvantages of catalytic photodegradation in batch system. Attempts to overcome this problem was made by immobilization of the photocatalyst as a thin film on different substrates [31]. Most titanium compounds are not water soluble and therefore, the precursors used for the synthesis of TiO_2 nanoparticles are limited and more expensive than other metal oxides. Most of magnesium compounds have good solubility in water and they are much cheaper. The synthesis of TiO_2 nanostructures need higher technology and more steps, which add further cost to its production.

In the present work, we have focused on the direct, template free and surfactant free synthesis of MgO nanostructure via direct precipitation of Mg^{2+} ions with a strong base and evaluating its efficiency as a photocatalyst for the degradation of a medical waste stain (methylene blue) under direct solar and UV light irradiation.

Materials and methods

Magnesium nitrate hexahydrate, sodium hydroxide, methylene blue, methanol, and hydrochloric acid were obtained from Merck, Germany. The chemicals used were of analytical reagent grade and used without further purification. Titanium dioxide (particles size 25 nm) was purchased from Cheng Du Micxy chemical Co. Ltd., China. Zinc oxide (particle size 10–30 nm) was obtained from SkySpring nanomaterials Inc., Houston, USA. Methylene blue ($C_{16}H_{18}ClN_3S$) ($\lambda_{max} = 665$ nm) was used as a model dye pollutant of clinical labs. The MB concentrations were measured using Cary 60 UV–Vis spectrophotometer from Agilent. 200 mg/L stock solution of MB was prepared and the working solutions were prepared by dilution with distilled water. The initial pH was adjusted with dilute HCl (0.1 M) or NaOH (0.1 M) using a pH-meter.

Synthesis of MgO-NPs

Magnesium oxide nanoparticles were synthesized using magnesium nitrate ($MgNO_3{\cdot}6H_2O$) as a source of Mg^{2+} ion with sodium hydroxide as the OH^- source. For the typical experimental procedure, 0.2 M $MgNO_3{\cdot}6H_2O$ was dissolved in 100 mL of distilled water. 0.5 M sodium hydroxide solution was added drop wise to the prepared magnesium nitrate solution with continuous stirring. The white precipitate of magnesium hydroxide appeared in beaker after few minutes. The stirring was continued for 60 min. Then the white precipitate was filtered and washed three times with methanol and distilled water and dried at 100 °C for 3 h. The dried powder was then crush to very fine powder using an agate mortar. Finally, the fine powder of MgO was obtained by calcination at 500 °C for 2 h.

Characterization

X-ray diffraction (XRD) analysis was recorded using A PANalytical X'Pert PRO diffractometer (Cu-$K_{\alpha 1}$ radiation $\lambda = 1.5406$ Å, generated at 40 kV and 40 mA). The samples were investigated from 2° to 80° 2θ with a step size of 0.0260° 2θ and a measuring time of 40 s/step. The surface morphology of the as-synthesized MgO-NPs was analyzed using scanning electron microscope (SEM) model MIRA3 TESCAN equipped with energy dispersive X-ray (EDX). The instrument was accelerated with a voltage of 30 kV. Cary 60 UV–Vis spectrophotometer was used to obtain the spectrum of the as-synthesized MgO-NPs in the range of 200–500 nm to estimate the optical band gap.

Photocatalytic degradation studies

For all the photocatalytic degradation experiments, an open top glass cell of cylindrical shape (15 cm diameter) was used. The cell was fixed inside a thin plastic dish that was thermally controlled with the aid of a chiller (water jacketed). The whole system was mounted on magnetic stirrer to face the light source (direct sunlight or UV source). Two UV light sources of 254 and 365 nm were provided using Chromato-Vue Cabinet, model C-75 (15 W, inner dimensions: 43 cm Length × 35 cm Width and 13 cm Height). Catalytic photodegradation studies were performed using 150 mL of the MB solution of 10 mg/L (except for the initial dye concentration study) and 0.1 g of the MgO-NPs (except for the catalyst dose study). In order to attain the adsorption–desorption equilibrium of methylene blue on MgO-NPs, the suspensions were stirred in the reactor in dark for 30 min. 4 mL aliquots were collected after 30 min in the dark, and after irradiation, at different time intervals for the kinetic studies. The portions were centrifuged (4500 rpm) for 10 min and from the absorbance (at 665 nm) of the supernatants, the concentration of the remained methylene blue were determined.

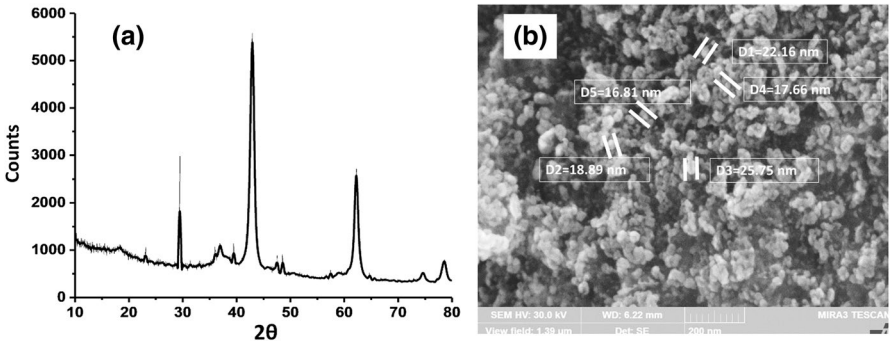

Fig. 1 X-ray diffraction pattern (**a**) and SEM image (**b**) of the MgO-NPs

Table 1 XRD data for particle size measurement

Peak position (2θ)	FWHM	Particle size (nm)
36.9	3.298	2.5
42.9	0.891	9.6
62.2	0.825	11.3
74.7	0.881	11.4
78.6	0.973	10.6

Medical lab wastewater treatment

The washing waste from the preparation of bacterial slides contains relatively high concentration of methylene blue (Leishman stain) [32]. The wastewater was collected from three clinical laboratories and diluted with distilled water (1:1). 150 mL of this real sample was introduced to the reaction vessel with 0.1 g of the MgO-NPs, stirred in dark for 30 min for adsorption–desorption equilibration then irradiated with direct sunlight for catalytic photodegradation process. Aliquots of the mixture were taken out at different time of the irradiation for analysis.

Results and discussion

Characterization of MgO-NPs

The crystal structure of the as-synthesized MgO-NPs was determined with powder XRD (Fig. 1a) which shows major reflections at 2θ = 36.91°, 42.94°, 62.20°, 74.68° and 78.58° corresponding to (111), (200), (220), (311) and (222) planes of MgO nano-cubes [33, 34]. Table 1 shows the main diffraction peaks that were used to calculate the average particle size of the nano-MgO using the Debye–Scherrer equation (Eq. 1) [35].

$$D = \frac{K\lambda}{\beta \cos\theta} \quad (1)$$

here K is a dimensionless shape factor ($K = 0.9$), λ is wavelength (nm) of the XRD, and β is full width at half maximum height (FWHM) of the diffraction peak at an angle θ (in Radians). The particle size distribution was observed in a narrow range between 2.54 and 11.35 nm (Table 1). The average particle size was found to be 9.06 nm.

The energy dispersive X-ray (EDX) image (Fig. S1) shows the presence of small percentage (2.03%) of Ca in addition to the main components (Mg = 47.65% and O = 50.31%). The SEM micrograph (Fig. 1b) shows small sized cubic MgO particles between 16.8 and 25.7 nm with an average size of 20.0 nm.

The optical band gap energy was estimated from the Tauc relation (Fig. S2) as 4.25 eV. Similar results were obtained for nano-MgO [36, 37]. Bulk MgO has a bandgap of 7.8 eV [38, 39]. The blue shift can be explained on the basis of very small size of the synthesized MgO-NPs as confirmed by the XRD results above.

The photoluminescence spectra (PL) of the dispersed MgO-NPs (Fig. 2) excited at 325 nm shows four emission peaks centered at 360, 494, 517 and 545 nm. The rapid evaporation and incomplete crystallization may generate various structural defects, contributing to the observed emissions in MgO nanoparticles. It has to be mentioned that bulk MgO does not show PL activity because MgO is a typical wide band gap insulator (7.8 eV) and it have low concentration of the native defects in bulk MgO [40]. The peaks centered at 360 and 517 nm corresponds to the F^+ and F oxygen vacancy defects that are vacancies containing one and two electrons respectively [41]. The high intensity emission peak at 360 nm may also be ascribed to the scattering from the voids between the nano-MgO particles. The higher the defect concentration, the higher the PL intensity [42].

Furthermore, a high concentration of native defects for MgO-NPs may result in the higher recombination of oxidative species and decrease of photoactivity.

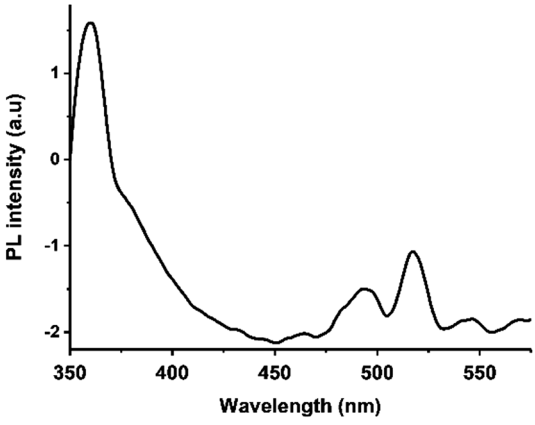

Fig. 2 Photoluminescence (PL) spectra of the as-synthesized MgO-NPs excited at 325 nm

As the photocatalytic activity occurs on the surface of the catalyst and the first step is likely to be an adsorption process, it is obvious that the surface area has a great role on the rate of the photocatalysis. Although in some studies no correlation was found between adsorption of dye and photocatalytic degradation [43].

Photocatalysis studies

It is important to study the kinetics of the photocatalytic degradation and the various effects governing the degradation rate to make the research applicable to environment. Fig. 3a shows the decrease in the intensity of the absorption spectra of MB vs irradiation time under direct sunlight. No detectable photo-degradation of MB was observed in the absence of the MgO-NPs under direct sunlight. Very low concentrations of the dye were used for the photodegradation studies, therefore pseudo first-order kinetic model was considered (Eq. 2) [44] using non-linear regression (Fig. 3b) with the aid of OriginPro software for estimation of the kinetic parameters (Table 2). The as-synthesized MgO-NPs was compared to nano-ZnO (10–30 nm) and nano-TiO_2 using different light sources (365 nm and 254 nm UV lamps of 10 W power, and direct sunlight). Evaluation of the as-prepared MgO-NPs as a

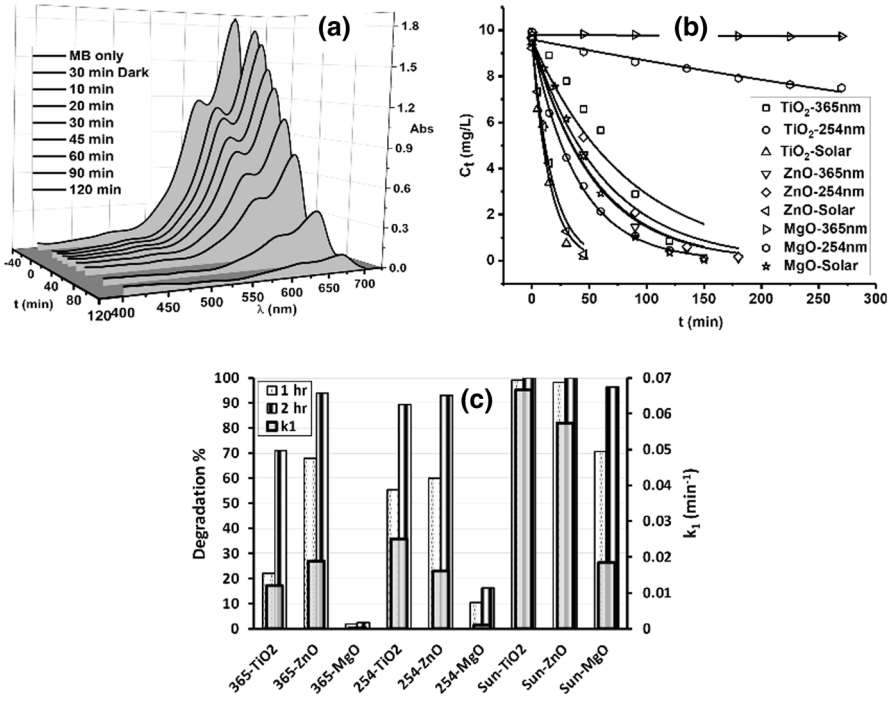

Fig. 3 Time dependent absorption spectra of MB (0.1 g MgO-NPs, pH 6.0, direct sunlight) (**a**), non-linear regression pseudo-first order kinetics (**b**) and k_1 and degradation % after 1 h and 2 h irradiation (**c**)

Table 2 Evaluation of photodegradation efficiency and pseudo first-order rate constants for MB using different photocatalyst and irradiation source

Radiation source	Photocatalyst	Degradation (%)	k_1 (min^{-1})	R^2
365 nm	TiO_2	71.1	$0.012 \pm 1.7 \times 10^{-3}$	0.908
	ZnO	94.0	$0.019 \pm 1.2 \times 10^{-3}$	0.993
	MgO	2.6	$2.7 \times 10^{-5} \pm 1.3 \times 10^{-5}$	0.390
254 nm	TiO_2	89.2	$0.025 \pm 4.0 \times 10^{-4}$	0.993
	ZnO	93.0	$0.016 \pm 1.4 \times 10^{-3}$	0.986
	MgO	16.2	$0.001 \pm 5.2 \times 10^{-5}$	0.959
Direct sunlight	TiO_2	100	$0.067 \pm 6.0 \times 10^{-3}$	0.978
	ZnO	100	$0.057 \pm 3.6 \times 10^{-3}$	0.987
	MgO	96.7	$0.018 \pm 1.5 \times 10^{-3}$	0.971

photocatalyst was done via the comparison of degradation % and pseudo first-order rate constants (Fig. 3c).

$$C_t = C_o e^{-k_1 t} \tag{2}$$

here C_o and C_t are the dye concentration initially and at t time passed over photodegradation respectively. At room temperature, the MgO-NPs under low energy photons of 365 nm shows very low degradation % and rate (k_1), while TiO_2 and ZnO nano-particles presented more than 70% degradation in 2 h. As the energy of the photons increased to 254 nm wavelength, MgO efficiency presented slightly better performance (Table 2), while under higher energy photons of direct sunlight, the nano-MgO showed comparable efficiency after 2 h irradiation but lower rate of degradation compared to nano-ZnO and TiO_2 photocatalyst (Fig. 3c). The comparison between different irradiation sources (energy of a photon) is reasonable if their total power applied on the surface of the reaction mixture were the same. About 1/4 of the UV irradiation from the source is directed to the bottom of the cabinet. The interior area of the cabinet and the cylindrical reaction cell are 0.15 m^2 and 0.0177 m^2 ($\approx$8:1) respectively. This shows that about 1/30 of the UV light touches the surface of the reaction mixture ($\approx$0.5 W). The UV part of the direct sunlight [12] is 20–30 W/m^2. The contact area with the reaction mixture is 0.0177 m^2. Thus, about 0.5 W UV energy reaches the surface of the mixture but contains wide range of UV frequencies.

It is reported that MB may transform to colorless leuco form (unstable) by taking photo-excited electrons with the action of UV light. The blue color of MB may reappear if the colorless sample exposed to air to form the oxidized blue MB [3]. To insure irreversible degradation, the samples (after photocatalytic experiments) were exposed to air overnight and no blue color appeared, which confirms the catalytic photodegradation process.

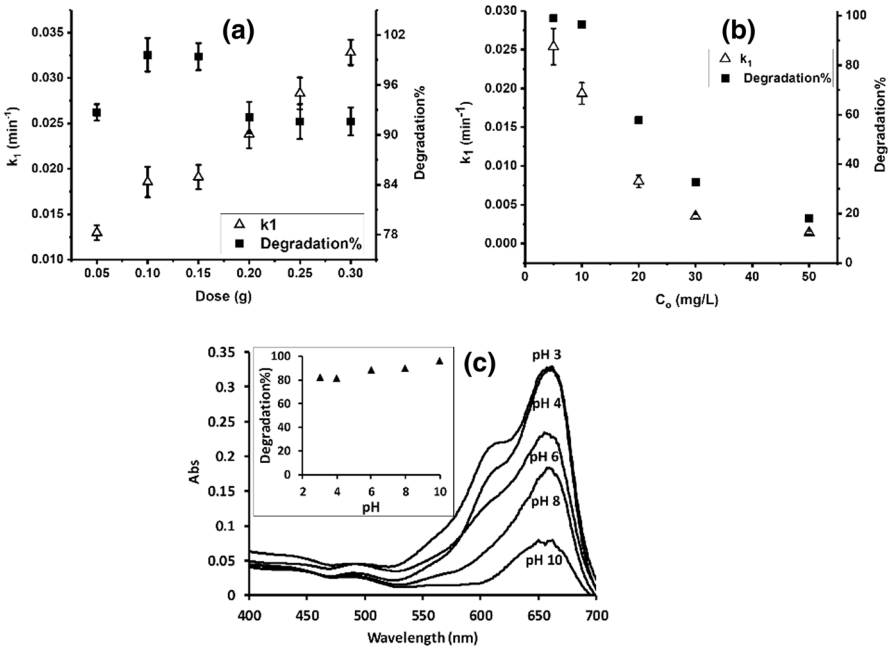

Fig. 4 Effect of catalyst dose (**a**), initial MB concentration (**b**) and initial pH (**c**) on the photocatalytic degradation efficiency of MB after 120 min irradiation of direct sunlight irradiation using 0.1 g MgO-NPs

Effect of operational parameters

The effects of photocatalyst dose (MgO-NPs), initial MB concentration, initial pH on the degradation % and k_1 were studied using 150 mL MB at room temperature (Fig. 4). The effect of MgO-NPs dose was studied in the range of 0.05 to 0.3 g. An increase of the percentage degradation and k_1 was observed with increasing the amount of MgO-NPs from 0.05 to 0.1 g probably due to the increase of the surface area of the photocatalyst and higher adsorption that leads to higher degradation percentage and rate (Fig. 4a). A further increase of the amount of MgO causes lowering of the degradation percentage slightly which may be due the formation of aggregates of MgO-NPs that cause lowering of the surface area and active sites. Another process that may contribute in lowering the efficiency is the restriction of light by higher amounts of the MgO-NPS [45].

The experiments were carried out using various initial concentration of MB (5–50 mg/L) to explore the effect of the initial concentration of MB. The degradation percentage and rate (k_1) decreased with increasing the initial concentration of MB (Fig. 4b). As the concentrations of the dye (MB) increase, significant amount of the solar light is likely absorbed by the MB molecules rather than the catalyst [46].

The photocatalytic activity was investigated at various initial pH from 3.0 to 11.0 (Fig. 4c). The results show a slight increase (80% to 97%) in the degradation efficiency of as the pH increased from 3.0 to 11.0 respectively. The change of the pH

has effect on the surface groups of the photocatalyst as it is related to the point of zero charge (PZC) and it determines the size of aggregates. The PZC of MgO is reported as 11.6 [47]. pH change has effect on the functional groups of dye molecules also which is related to the pK_a values of the dye. Below pH 11.6, where pH < PZC (as in the present case), the MgO-NPS surface would be positively charged. Increasing pH reduces the positive charge on the surface of the MgO-NPs and hence decreasing electrostatic repulsion between the cationic MB molecules and the MgO-NPs surface. Increasing pH enhances $OH^{\cdot}$ generation [48].

The effect of temperature on the rate constant (k_1) is better reflected by the activation energy, which is in turn estimated from the Arrhenius equation (Eq. 3). The rate constant at 298 and 318 K were determined from their kinetic plots (Fig. S4), from which the activation energy was estimated using the integrated form of Arrhenius equation (Eq. 4).

$$k = Ae^{-E_a/RT} \tag{3}$$

$$\frac{\ln k_2}{\ln k_1} = -\frac{E_a}{R}\frac{T_2}{T_1} \tag{4}$$

here E_a is the activation energy and A is the pre-exponential factor. The activation energy was found to be 32.9 kJ/mol, which is very close (but slightly higher) to the values of catalytic photodegradation of MB using TiO_2 photocatalyst under UV. The mechanism by which organic pollutants decompose through hydroxyl radical reaction have comparable activation energies. This suggests a reaction mechanism that is controlled by hydroxyl radical reaction [3, 49].

Application on real samples

Medical laboratories (hematology or histopathology) use different stains to develop distinguishable color in the cell under investigation. The cells maybe bacteria, blood cells or bone marrow. Traditionally, a glass slide is covered with a thin layer of the specimen (i.e. blood) and dried at room temperature. Then few drops of the stain are applied to the slide and washed with distilled water after 2–3 min. The wastewater of three laboratories were collected and their mixture was used as a real sample for catalytic photodegradation experiments. The concentration of MB of the wastewater sample was 33 mg/L. The sample was diluted (1:1 with distilled water) to become 16.5 mg/L. The MB concentration has reduced to 16.2 mg/L (1.3% removal) after equilibrium adsorption in dark place for 30 min and then to 0.35 mg/L (97.8% degradation) after 2 h of solar irradiation (S 5).

Conclusion

MgO-NPs was synthesized by a simple chemical precipitation method without the use of template or surfactant. The particle size distribution of the MgO-NPs was between 2.5 and 11.35 nm. 4.25 eV was observed for the optical band gap energy.

Photocatalytic experiments showed that the as-synthesized MgO-NPs have good efficiency compared to ZnO and TiO_2 nanoparticles using direct solar irradiation. The photocatalytic activity was attributed to the presence of native F and F^+ oxygen vacancy defects at the surface of the MgO-NPs. The optimum catalytic photoactivity was at low concentration of the dye while initial pH has small effect on the efficiency of degradation. 97.8% photodegradation of 1:1 diluted medical lab wastewater was achieved in 2 h of direct irradiation of sunlight using the as-synthesized MgO-NPs. The current study shows that direct sunlight can be used as a powerful renewable source of radiation to degrade various organic pollutant without the need of high technology or cost effective equipment.

Compliance with ethical standards

Conflicts of interest The authors declare that they have no conflict of interest.

References

1. Abbasi M, Asl NR (2008) Sonochemical degradation of basic blue 41 dye assisted by nano TiO_2 and H_2O_2. J Hazard Mater 153:942–947
2. Yue QF, Xiong B, Chen WX, Liu XY (2014) Comparative study of the efficacy of Wright–Giemsa stain and Liu's stain in the detection of Auer rods in acute promyelocytic leukemia. Acta Histochem 116:1113–1116
3. Yi-Hsuan C, Tso-Fu CM, Chun-Yi C, Masato S, Yung-Jung H (2019) Mechanistic insights into photodegradation of organic dyes using heterostructure photocatalyst. Catalysts 9:430. https://doi.org/10.3390/catal9050430
4. Dingwang C, Sivakumar M, Ajay RK (2000) Heterogeneous photocatalysis in environmental remediation. Dev Chem Eng Miner Process 8(5/6):505–550
5. Yin H, Qiu P, Qian Y, Kong Z, Zheng X, Tang Z, Guo H (2019) Textile wastewater treatment for water reuse: a case study. Processes 7(1):34. https://doi.org/10.3390/pr7010034
6. Salh DM, Aziz BK, Kaufhold S (2019) High adsorption efficiency of Topkhana natural clay for methylene blue from medical laboratory wastewater: a linear and nonlinear regression. Silicon. https://doi.org/10.1007/s12633-019-00100-0
7. Zhou D, Liu X, Chen C (2019) harmless treatment of phenylhydrazine hydrochloride production effluent: from lab scale to pilot scale. Water 11:608. https://doi.org/10.3390/w11030608
8. Rajasulochana P, Preethy V (2016) Comparison on efficiency of various techniques in treatment of waste and sewage water—a comprehensive review. Resour-Effic Technol 2:175–184
9. Alvarino T, Suarez S, Lema J, Omil F (2018) Understanding the sorption and biotransformation of organic micropollutants in innovative biological wastewater treatment technologies. Sci Total Environ 615:297–306
10. Venkatesh S, Venkatesh K, Quaff A (2017) Dye decomposition by combined ozonation and anaerobic treatment: cost effective technology. J Appl Res Technol 15:340–345
11. Subrata N, Arumugom SP, Manas C (1998) Photocatalytic degradation of organic dyes in aqueous solution with TiO_2 nanoparticles immobilized on foamed polyethylene sheet. J Photochem Photobiol A 113:257–264
12. Akira F, Xintong Z, Donald TA (2007) Heterogeneous photocatalysis: from water photolysis to applications in environmental cleanup. Int J Hydrog Energy 32:2664–2672
13. Lean J, Rind D (1998) Climate forcing by changing solar radiation. J Clim 11:3069–3094
14. Dong H, Zeng G, Tang L, Fan C, Zhang C, He X, He Y (2015) An overview on limitations of TiO_2-based particles for photocatalytic degradation of organic pollutants and the corresponding countermeasures. Water Res 79:128–146

15. Gomes J, Lincho J, Domingues E, Quinta-Ferreira RM, Martins RC (2019) N-TiO2 photocatalysts: a review of their characteristics and capacity for emerging contaminants removal. Water 1:373. https://doi.org/10.3390/w11020373
16. Emeline AV, Kuzmin GN, Basov LL, Serpone N (2005) Photoactivity and photoselectivity of a dielectric metal-oxide photocatalyst (ZrO_2) probed by the photoinduced reduction of oxygen and oxidation of hydrogen. J Photochem Photobiol A 174:214–221
17. Behnajady MA, Moghaddam SG, Modirshahla N, Shokri M (2009) Investigation of the effect of heat attachment method parameters at photocatalytic activity of immobilized ZnO nanoparticles on glass plate. Desalination 249:1371–1376
18. Han F, Kambala VS, Srinivasan M, Rajarathnam D, Naidu R (2009) Tailored titanium dioxide photocatalysts for the degradation of organic dyes in wastewater treatment: a review. Appl Catal A 359:25–40
19. Show B, Mukherjee N, Mondal N (2016) α-Fe_2O_3 nanospheres: facile synthesis and highly efficient photo-degradation of organic dyes and surface activation by nano-Pt for enhanced methanol sensing. RSC Adv 6:75347–75358
20. Sathyamoorthy R, Mageshwari K (2013) Synthesis of hierarchical CuO microspheres: photocatalytic and antibacterial activities. Physica E 47:157–161
21. Cruz AM, Martinez DS, Cuellar EL (2010) Synthesis and characterization of WO3 nanoparticles prepared by the precipitation method: evaluation of photocatalytic activity under vis-irradiation. Solid State Sci 12:88–94
22. Zheng Y, Cao L, Xing G, Bai Z, Huanga J, Zhang Z (2019) Microscale flower-like magnesium oxide for highly efficient photocatalytic degradation of organic dyes in aqueous solution. RSC Adv 9:7338–7348
23. Mantilaka MMMG, De Silva RT, Ratnayake SP, Amaratunga G, de Silva KMN (2018) Photocatalytic activity of electrospun MgO nanofibres: synthesis, characterization and applications. Mater Res Bull 99:204–210
24. Alvarez M, López T, Odriozola JA, Centeno MA, Dominguez MI, Montes M, Quintana P, Aguilar DH, Gonzalez RD (2007) 2,4-Dichlorophenoxyacetic acid (2,4-D) photodegradation using an Mn^+/ZrO_2 photocatalyst: XPS, UV–vis, XRD characterization. Appl Catal B 73:34–41
25. Sutradhar N, Sinhamahapatra A, Pahari SK, Pal P, Bajaj HC, Mukhopadhyay I, Panda AB (2011) Controlled synthesis of different morphologies of MgO and their use as solid base catalysts. J Phys Chem C 115:12308–12316. https://doi.org/10.1021/jp2022314
26. Gedanken A (2004) Using sonochemistry for the fabrication of nanomaterials. Ultrason Sonochem 11:47–55
27. Karthik K, Dhanuskodi S, Gobinath C, Prabukumar S, Sivaramakrishnan S (2019) Fabrication of MgO nanostructures and its efficient photocatalytic, antibacterial and anticancer performance. J Photochem Photobiol B 190:8–20
28. Wang H, Rogach AL (2014) Hierarchical SnO_2 nanostructures: recent advances in design, synthesis, and applications. Chem Mater 26(1):123–133
29. Pudukudy M, Yaakob Z, Rajendran R, Kandaramath T (2014) Photodegradation of methylene blue over novel 3D ZnO microflowers with hexagonal pyramid-like petals. Reac Kinet Mech Cat 112:527–542. https://doi.org/10.1007/s11144-014-0703-5
30. Zhang Z, Zheng Y, Chen J, Zhang Q, Ni Y, Liang X (2007) Facile synthesis of monodisperse magnesium oxide microspheres via seed-induced precipitation and their applications in high-performance liquid chromatography. Adv Funct Mater 17:2447–2454
31. Kerkez Ö, Boz İ (2013) Efficient removal of methylene blue by photocatalytic degradation with TiO_2 nanorod array thin films. Reac Kinet Mech Cat 110:543–557. https://doi.org/10.1007/s11144-013-0616-8
32. Ahmed HR, Raheem SJ, Aziz BK (2017) Removal of Leishman stain from aqueous solutions using natural clay of Qulapalk area of Kurdistan region of Iraq. Karbala Int J Mod Sci 3:165–175. https://doi.org/10.1016/j.kijoms.2017.05.002
33. Mageshwari K, Sathyamoorthy R (2012) Preparation and characterization of MgO nanoflakes by wet precipitation method. In: Proceedings of national conference on developing scenario in applied sciences and communicative english, pp 56–58
34. Dhal JP, Sethi M, Mishra BG, Hota G (2015) MgO nanomaterials with different morphologies and their sorption capacity for removal of toxic dyes. Mater Lett 141:267–271
35. Tamilselvi P, Yelilarasi A, Hema M, Anbarasan R (2013) Synthesis of hierarchical structured MgO by sol-gel method. Nano Bull 2:1

36. Sohrabi L, Taleshi F, Sohrabi R (2014) Effect of carbon nanotubes support on band gap energy of MgO nanoparticles. J Mater Sci 25:4110–4114
37. Kamarulzaman N, Chayed NF, Badar N, Kasim MF, Mustaffa DT, Elong K, Rusdi R, Oikawa T, Furukawa DT (2016) Band gap narrowing of 2-D ultra-thin MgO graphene-like sheets. ECS J Solid State Sci Technol 5(11):Q3038–Q3045
38. Taurian OE, Springborg M, Christensen NE (1985) Self-consistent electronic structures of MgO and SrO. Solid State Commun 55(4):351–355
39. Wobbe M, Kerridge A, Zwijnenburg M (2014) Optical excitation of MgO nanoparticles: a computational Perspective. Phys Chem Chem Phys 16(40):22052–22061. https://doi.org/10.1039/c4cp03442b
40. Mageshwari K, Mali SS, Sathyamoorthy R, Patil PS (2013) Template-free synthesis of MgO nanoparticles for effective photocatalytic applications. Powder Technol 249:456–462
41. Deepak FL, Saldanha P, Vivekchand SRC, Govindaraj A (2006) A study of the dispersions of metal oxide nanowires in polar solvents. Chem Phys Lett 417:535–539
42. Janet CM, Viswanathan B, Viswanath RP, Varadarajan TK (2007) Characterization and photoluminescence properties of MgO microtubes synthesized from hydromagnesite flowers. J Phys Chem C 111:10267–10272
43. Guo MY, Ching Ng AM, Liu F, Djurisic AB, Chan WK (2011) Photocatalytic activity of metal oxides—the role of holes and OH· radicals. Appl Catal B 107:150–157
44. Saai Harini R, Easwaramoorthy D, Sai Muthukumar V, Gowrishankar R (2019) Highly efficient band engineered tin—carbon codoped bismuth titanate nanowires for visible light photocatalytic application. Environ Nanotechnol Monit Manag. https://doi.org/10.1016/j.enmm.2019.100228
45. Amalraj A, Pius A (2015) Photocatalytic degradation of monocrotophos and chlorpyrifos inaqueous solution using TiO_2 under UV radiation. J Water Process Eng 7:94–101
46. Rajamanickam D, Shanthi M (2016) Photocatalytic degradation of an organic pollutant by zinc oxide—solar process. Arab J Chem 9:1858–1868
47. Bera S, Udayabhanu G, Narayan R, Rout TK (2013) Sol-Gel Process for Anti-Corrosion Coatings. J Res Updates Polym Sci 2:209–231
48. Yang C, Dong W, Cui G, Zhao Y, Shi X, Xia X, Tang B, Wang W (2017) Highly-efficient photocatalytic degradation of methylene blue by PoPD-modified TiO_2 nanocomposites due to photosensitization-synergetic effect of TiO_2 with PoPD. RSC Adv 7:23699–23708
49. Wu CH, Chern JM (2006) Kinetics of photocatalytic decomposition of methylene blue. Ind Eng Chem Res 45:6450–6457

Publisher's Note Springer Nature remains neutral with regard to jurisdictional claims in published maps and institutional affiliations.